

EXPRESS LETTER

Open Access



On the genesis of multi-peak vertical structure of quasi-two-day waves in the mesosphere–lower thermosphere

S. S. Prijith^{1*}  and K. Kishore Kumar¹

Abstract

The study presents multi-peak vertical structure of westward propagating quasi-two-day wave with wave-number 3 (W3) and its formation mechanisms in the mesosphere–lower thermosphere, using two decades of multi-satellite measurements, for the first time. W3 in austral summer shows a multi peak vertical structure, with two prominent peaks having amplitudes of 11.24 ± 2.2 K and 8.66 ± 1.1 K at 108 km (M1) and 84 km (M2), respectively. Genesis of this multi-peak structure, which is not explored in details hitherto, is investigated. While weak eastward/westward winds favour vertical growth of W3 in the regions of M1 and M2, strong eastward winds weaken W3 in the region between M1 and M2. These changes in zonal winds are modulated by the altitude variations in meridional temperature gradient and gravity wave filtering. Thus, vertically alternating changes in wind and meridional temperature gradient are the potential drivers for the multi-peak vertical structure of W3, which will be of importance for atmosphere–ionosphere coupling processes.

Keywords Quasi-two-day wave, Mesosphere–lower thermosphere, W3 vertical structure, SABER, TIDI

*Correspondence:

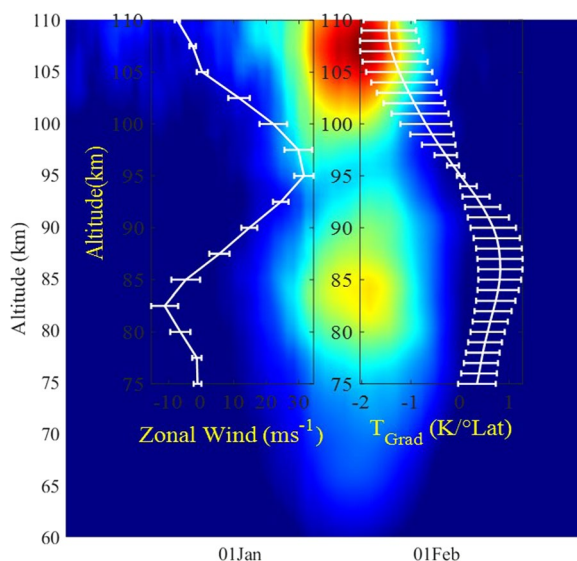
S. S. Prijith
prijithss@gmail.com

Full list of author information is available at the end of the article



© The Author(s) 2023. **Open Access** This article is licensed under a Creative Commons Attribution 4.0 International License, which permits use, sharing, adaptation, distribution and reproduction in any medium or format, as long as you give appropriate credit to the original author(s) and the source, provide a link to the Creative Commons licence, and indicate if changes were made. The images or other third party material in this article are included in the article's Creative Commons licence, unless indicated otherwise in a credit line to the material. If material is not included in the article's Creative Commons licence and your intended use is not permitted by statutory regulation or exceeds the permitted use, you will need to obtain permission directly from the copyright holder. To view a copy of this licence, visit <http://creativecommons.org/licenses/by/4.0/>.

Graphical Abstract



Introduction

Quasi-two-day wave (QTDW) is one of the most prominent planetary scale waves in the mesosphere–lower thermosphere (MLT) region of the Earth’s atmosphere (Muller and Kingsley 1974; Salby 1981a; Vincent 2015). QTDW is reported to be the manifestation of westward propagating gravest normal mode of Rossby-gravity wave with wave number 3 (Salby and Roper 1980; Salby 1981a). It is also reported that QTDW is generated due to baroclinic instability of summer easterly jet in the mesosphere (Pfister 1985; Plumb 1983). QTDWs intensify after summer solstice in both the hemispheres (Harris and Vincent 1993; Jacobi et al. 1997, 1998; Pancheva et al. 2004; Yue et al. 2012a). However, QTDW in southern hemisphere in austral summer is stronger, compared to that in northern hemisphere in boreal summer (Tunbridge et al. 2011; Yue et al. 2012a). Thus, dynamics of MLT region in southern hemisphere in summer is dominated by QTDW (Vincent 2015). Though QTDW manifests in several modes with different wave numbers, in westward and eastward directions, westward propagating one with wave number 3 (hereafter this component of QTDW is referred as W3) in summertime southern hemisphere is the strongest among all of them (Gu et al. 2013, 2019; Huang et al. 2013; Tunbridge et al. 2011). Realizing the importance of QTDWs, several studies were carried out to characterize these waves and investigate their effects

in the middle atmosphere using model simulations (Palo et al. 1999; Yue et al. 2012a) and ground-based (Guharay et al. 2013; Kumar et al. 2018; Suresh Babu et al. 2011; Thayaparan et al. 1997) and space-based (Gu et al. 2013; Huang et al. 2013; Moudden and Forbes 2014; Pancheva et al. 2018) observations.

QTDWs play a key role in atmosphere–ionosphere coupling and affect ionospheric composition and processes (Pancheva 2006; Yue et al. 2012b, 2016). QTDW penetrate into regions of lower thermosphere, affect prevailing neutral winds and thereby alter the electric fields generated through dynamo mechanism (Moudden and Forbes 2014). But, penetration of QTDW to higher altitudes is controlled by prevailing zonal wind conditions in the middle atmosphere (He et al. 2021). However, there are other mechanisms, such as non-linear interaction with other atmospheric waves, including tides, through which QTDW can affect ionosphere (Yue et al. 2016). Secondary waves generated through these non-linear interactions can propagate further up and affect higher altitude regions (Nguyen et al. 2016). Hence, examining the altitude structure of QTDW and its variation is important to understand the coupling processes between lower and upper atmosphere. Strength of QTDW and its effects on atmosphere–ionosphere coupling are significantly influenced by atmospheric phenomena such as sudden stratospheric warming (SSW). During SSW

events, perturbations in Equatorial Electro Jet (EEJ) are reported due to modulations of lunar tides by QTDW (Li et al. 2021).

Earlier studies demonstrated importance of QTDW in shaping the structure and dynamics of middle atmosphere through different pathways as well as in atmosphere–ionosphere coupling. However, owing to scarcity in observations of atmospheric parameters in the MLT regions, many observational studies are limited up to 100 km altitude and thus hindering the comprehensive investigations on the vertical coupling processes. Using simulations from Thermosphere–Ionosphere–Mesosphere–Electrodynamics General Circulation Model (TIME-GCM) up to 160 km, Palo et al. (1999) reported a bimodal vertical structure of the QTDW amplitudes in the temperature fields with peaks at 82 and 105 km over southern high latitudes. Ward et al. (1996) also reported a bimodal structure of QTDW, but in zonal (peaking at 90 and 110 km) and meridional (peaking at 90 and 115 km) winds. Though there are numerous studies on QTDW over the past four decades focusing on several aspects of these waves such as their source mechanisms, propagating characteristics, wave-mean flow and wave-wave interactions, there are very limited investigations on the multi-peak vertical structure of QTDW and its generation mechanisms. The central objective of the present study is to investigate the multi-peak vertical structure of QTDW and to discuss its potential formation mechanisms, using two decades of TIMED/SABER and TIMED/TIDI observations over southern hemispheric high latitudes during austral summer.

Data and methodology

Vertical structure of W3 and its formation mechanisms are examined in this study, using kinetic temperature measurements from Sounding of Atmosphere using Broadband Emission Radiometry (SABER) and wind measurements from Timed Doppler Imager (TIDI) onboard the Thermosphere Ionosphere Mesosphere Energetics and Dynamics (TIMED) satellite, for a period of 20 years from 2002 to 2022. TIMED orbits the Earth in a near polar orbit at an altitude of 625 km and inclination of 74.1°. SABER is a limb scanning radiometer, having 10 channels covering the spectral range from 1.27 to 17 μm , which provides near global measurements of kinetic temperature and gas volume mixing ratios from stratosphere to lower thermosphere (Russell et al. 1999). TIDI is a limb scanning Fabry–Perot interferometer, which provides neutral wind measurements in the mesosphere and thermosphere by measuring the Doppler characteristics of OI 557.7 nm and rotational lines in the O₂ (0–0) band at 762 nm (Killeen et al. 1999). Amplitude of W3 is

estimated, using kinetic temperature measurements from SABER, by performing a least square fit method. This method has been developed for extracting wave characteristics from spatially and temporally irregular data (Gu et al. 2013; Wu et al. 1995). This methodology relies on the concept that the travelling planetary waves at a location at a given time can be represented as sum of sine and cosine functions as,

$$y = A\cos(2\pi(ft + S\lambda)) + B\sin(2\pi(ft + S\lambda)), \quad (1)$$

where f is frequency in cycles per day (cpd), S is wave number (in cycles per longitude circle), t is time and λ is longitude of measurement. Here, westward propagating waves are represented by positive values of S and eastward propagating waves are represented by negative values of S . SABER measurements at different locations at different time are used in Eq. (1) and values of A and B are obtained using the least square best fit method. Using the values of A and B , amplitude of the wave is computed as

$$\text{Amp} = \sqrt{A^2 + B^2}. \quad (2)$$

To perform the analysis, TIMED/SABER measurements of kinetic temperature are gridded at a horizontal resolution of 5° latitude \times 5° longitude and vertical resolution of 1 km. A sliding window of 8 days, which advances by a day, is considered for the computation of W3 amplitudes. Amplitude of a wave estimated by this method, using spatially and temporally irregular satellite measurements, can have aliasing effects from other waves, especially at higher latitudes (Gu et al. 2013; Moudden and Forbes 2014). Estimated amplitudes of W3 can have contributions from eastward propagating QTDW with wave number 2, due to aliasing effect, which has been discussed in earlier studies (Gu et al. 2013; Moudden and Forbes 2014).

Results and discussions

Vertical structure of W3 component of QTDW and its inter-annual variability

Strong events of QTDW in southern hemispheric mesosphere occur in mid-latitude regions during austral summer (Huang et al. 2013). Among many zonal wave numbers of QTDW, W3 component is found to be strongest in austral summer over the mid-latitude regions of southern hemisphere. Figure 1a depicts latitude–altitude variation of W3 in austral summer, averaged for the 20 years of study period from 2002 to 2022. Substantiating earlier reported observations, prominence of W3 in the mid-latitude regions, especially between 50° S and 20° S, is evident in the figure. Figure 1b shows vertical

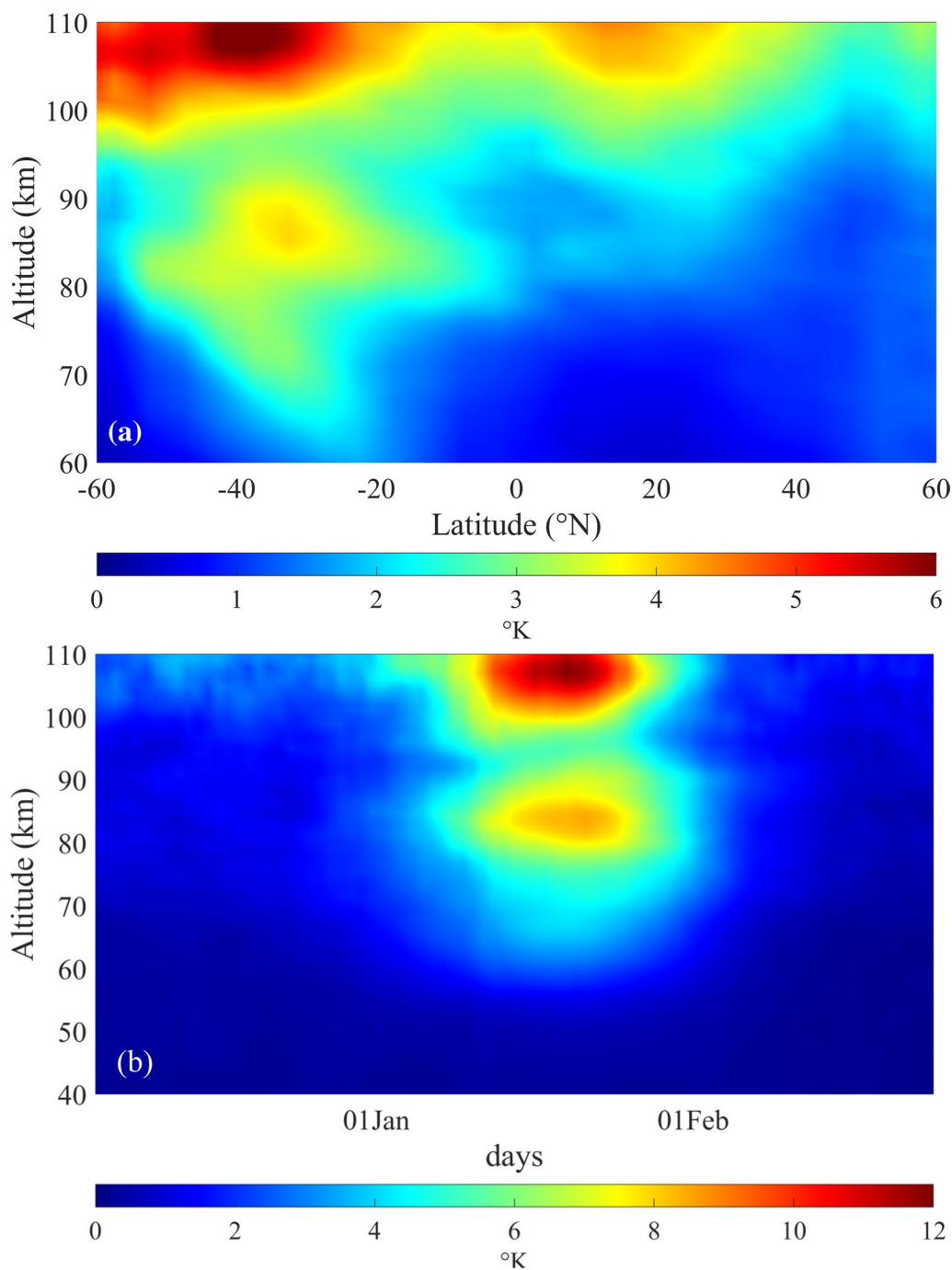


Fig. 1 **a** Mean latitude–altitude cross section of QTDW-W3 in austral summer during the period from 2002–03 to 2021–22. **b** Mean vertical structure of QTDW-W3 over the latitude band between 50° and 20° S in austral summer during the same period

structure of W3 over the latitude band between 50° S and 20° S, during austral summer, averaged for all the 20 years of study period. It was reported in earlier studies that QTDW starts strengthening after summer solstice (Harris and Vincent 1993; Jacobi et al. 1997, 1998; Pancheva et al. 2004). The present analysis also corroborates the

same, by showing enhancement in amplitudes of W3 in the month of January, as depicted in Fig. 1b. It is interesting to notice a multi-peak vertical structure of W3, with two prominent modes and one subtle mode. Prominent modes are observed to be at higher altitudes; one is above 100 km (peaking at 108 km) and another one is

above 80 km (peaking at 84 km), which are represented as M1 and M2, respectively, in the manuscript hereafter. In addition, a relatively weaker mode (M3) is observed at lower altitude levels above 60 km. Gu et al. (2019) have reported occurrence of M2 and M3 in Sudden Stratosphere Warming (SSW) years of 2006 and 2011. However, the weaker W3 mode above 60 km is reported to be not directly related to the strength of the wave and is evident mainly during the years of sudden stratospheric warming events (Gu et al. 2019). Increase in amplitudes of waves with increase in altitude is expected, in general, as the atmospheric density decreases with height. However, W3 amplitude is observed to be weakening at the altitude levels between 90 and 100 km and this leads to the formation of two prominent peaks at altitudes above and below this level. Using satellite-based wind measurements during January 19–31 in 1993, Ward et al. (1996) reported peak amplitude of QTDW at 94 km and a secondary maximum at 115 km over the region from 71° S to 41° N. During the same period, ground-based radar measurements also showed a double peak vertical

structure of QTDW in meridional wind, with a stronger peak at 110 and weaker one 125 km (Zhou et al. 1997). However, both of these studies are based on the measurements in the altitudes above 90 km, for a short period of less than 2 weeks. Present study, using 20 years of satellite measurements, shows additional peaks of QTDW in the MLT region, which were not reported in the above-mentioned studies. Based on the simulations carried out with TIME-GCM, Palo et al. (1999) reported a double peak vertical structure of W3 in temperature fields at 57.5° S, with peaks at 82 km and 105 km. The model simulations show larger amplitude for the upper peak, compared to that of the lower peak. Corroborating this inference from the model simulations, our analysis using two decades of satellite measurements show larger amplitude of W3 corresponding to M1, as compared to M2, over a larger spatial domain of southern hemisphere. Altitudes at which W3 amplitude peaks in M1 and M2 also show excellent agreement with the model simulated results by Palo et al. (1999).

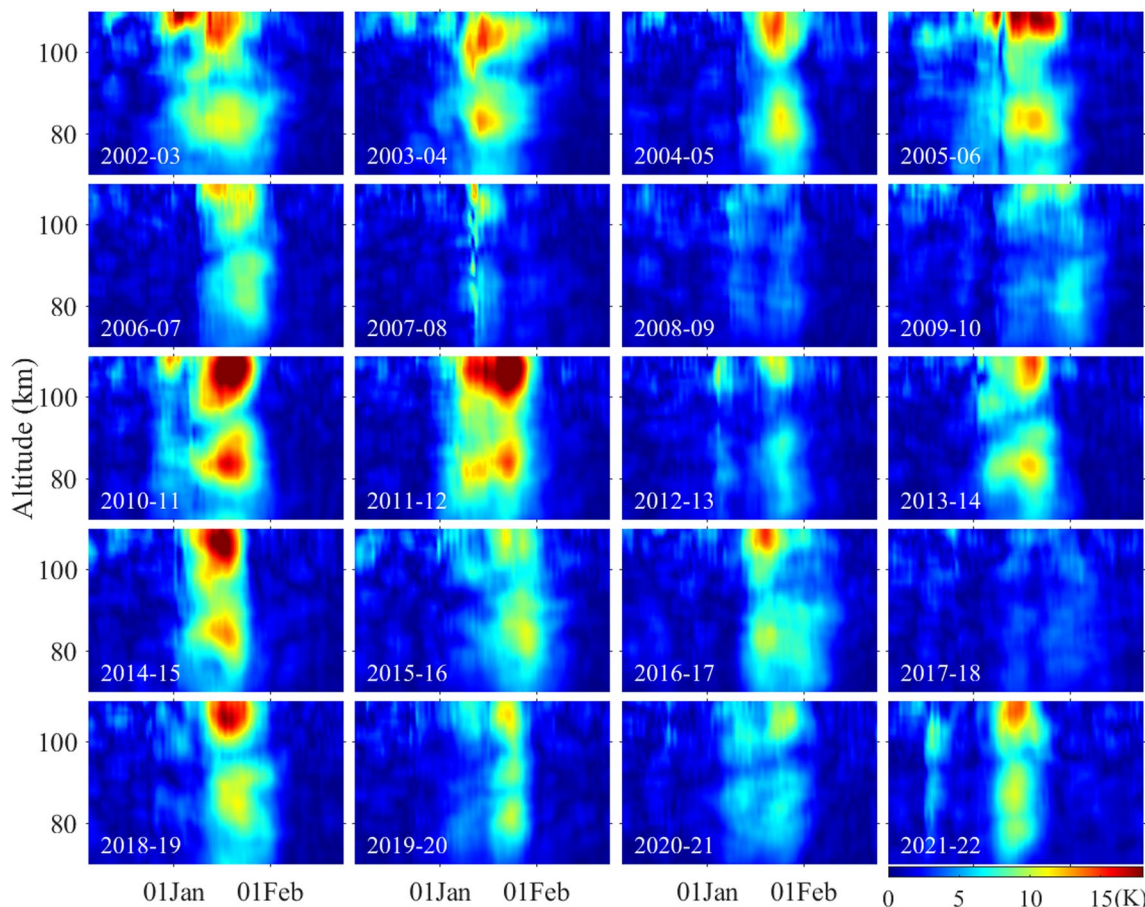


Fig. 2 Mean vertical structure of W3, over the latitude band between 50° and 20°S during the austral summer (December–February), for a period 20 years from 2002–03 to 2021–22

Further analysis is carried out to examine the consistency of W3 vertical structure in the MLT region in different years. Figure 2 shows the amplitudes of W3 in the altitude region between 70 and 110 km, averaged over the latitude band between 50° S and 20° S, during austral summer in all the 20 years from 2002 to 2022. Though significant inter-annual variability is observed in the strength of W3, the double-mode vertical structure

and weakening of W3 in the altitude region between the modes are consistently seen in all the years of W3 occurrence. Hence, further analysis has been carried out by examining the mean amplitudes in the regions of M1 and M2 in January in all the years from 2003 to 2022, as shown in Fig. 3a, b, respectively. While, Fig. 3a shows the mean amplitude of W3 in the region between 100 and 110 km (representing M1), Fig. 3b shows the same

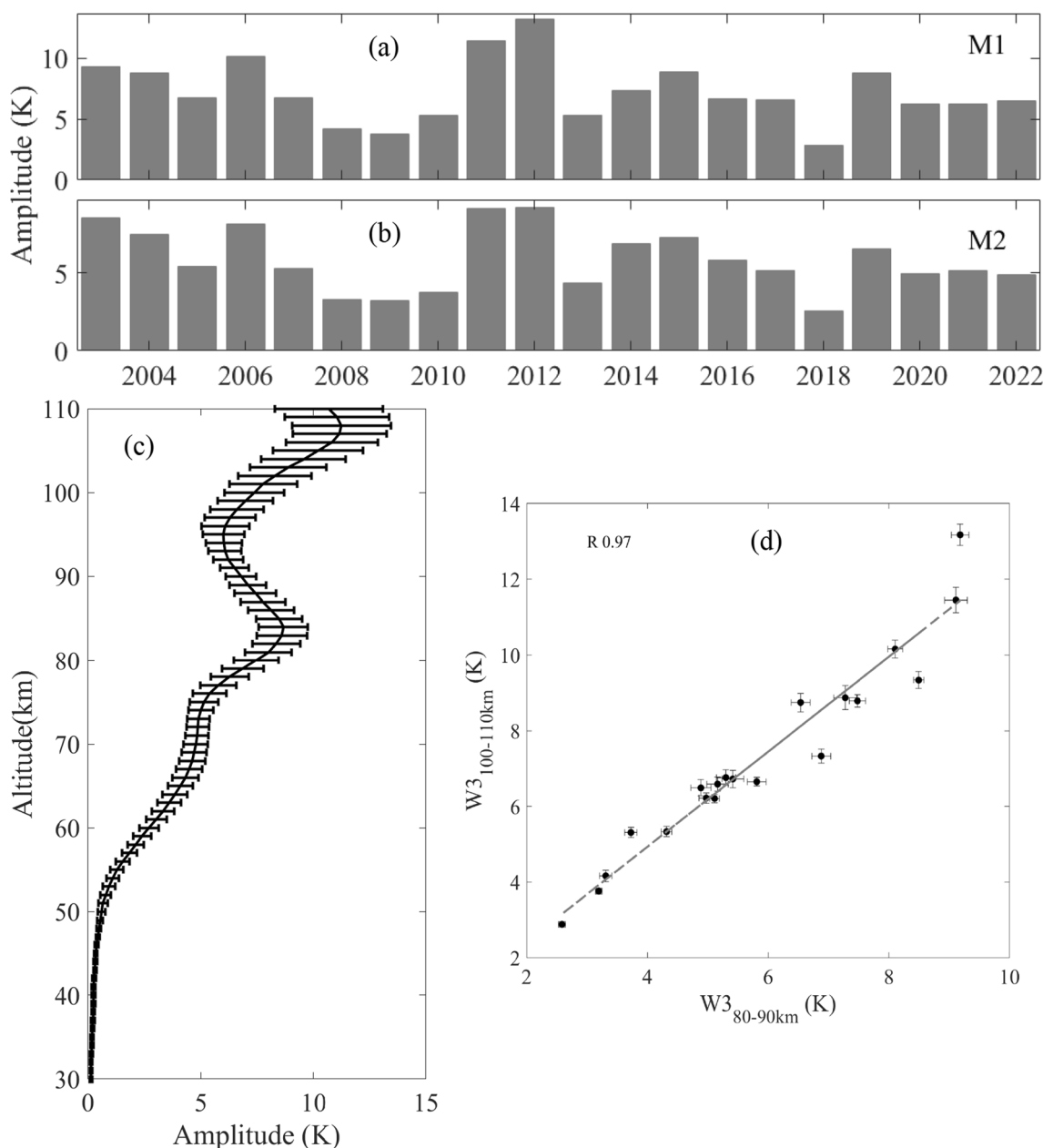


Fig. 3 Mean W3 amplitude corresponding to **a** M1 (100–110 km) and **b** M2 (80–90 km) in January from 2003 to 2022, averaged over the latitude band between 50° S and 20° S. **c** Mean vertical profile of W3 amplitude for the selected 8 years of strong W3 events, with horizontal bars representing standard deviations and **d** correlation between M1 and M2 amplitudes from all the years

in the region between 80 and 90 km (representing M2). Among all the years, strongest W3 event is observed in 2012, with mean amplitude of 13.17 K in region of M1 (100–110 km) and that of 9.18 K in the region of M2 (80–90 km). The vertical structure of W3 amplitudes in January, by considering the years of strong events (2003, 2004, 2006, 2011, 2012, 2014, 2015 and 2019), is shown in Fig. 3c. These are the years when the mean amplitude corresponding to M2 is greater than 70% of its highest amplitude observed in the year of 2012. The profile shows peak W3 amplitude of 11.24 ± 2.2 K (mean \pm standard deviation) at an altitude of 108 km, corresponding to M1. However, W3 amplitude corresponding to the peak of M2 is observed to be 8.66 ± 1.1 K at an altitude of 84 km. These values of W3 amplitudes, averaged over a larger spatial and temporal domain, are found to be very close to the TIME-GCM simulated amplitudes of 10 to 15 K at 57.5° S by Palo et al. (1999). To examine whether M1 and M2 are inter-dependent or not, correlation analysis is carried out as shown in Fig. 3d. The figure shows correlation between mean amplitudes of W3 in January in the altitude range 80–90 km and 100–110 km, from all the 20 years. It is evident from the figure that both the modes co-vary with a correlation coefficient of 0.97, thus ensuring the same source for the generation of both of the observed modes.

Vertical structure of temperature and zonal winds

Prevailing wind and temperature conditions can significantly influence the vertical propagation and hence the vertical structure of QTDW. To examine the causative mechanisms for the formation of double peak vertical structure of W3 in the MLT region, altitude profiles of zonal winds are examined in detail. Figure 4a shows the vertical structure of W3, averaged over the latitude band between 50° S and 20° S, in the month of January for all the years from 2003 to 2022 and Fig. 4b shows the vertical structure of zonal winds, estimated from TIDI measurements, averaged over the same region in January during the period from 2003 to 2020. While the double-mode vertical structure of W3 is evident in Fig. 4a in the years of strong events, an alternating vertical structure of zonal winds is seen in Fig. 4b in the MLT region. Coinciding with the regions of W3 weakening (shown in Fig. 4a), strong eastward winds are observed in the altitude range between 90 and 100 km (shown in Fig. 4b). However, zonal winds are found to be westward in the altitude regions above and below this layer of strong eastward winds. Further analysis has been carried out by considering the vertical profiles of zonal winds in the years of strong W3 occurrence. Figure 5a depicts vertical profile of zonal mean zonal winds in the month of January from the above-mentioned 8 years of strong W3 events, over

the latitude regions between 50° S and 20° S. As shown in the figure, zonal winds exhibit vertically alternating structure with weak westward winds at lower (below 85 km) and upper levels (above 105 km) of the MLT region and relatively stronger eastward winds in the altitude regions in between. Eastward wind is observed to be strongest at ~ 95 km, with amplitude greater than 25 m/s. However, weak westward/eastward winds are seen at the altitude levels of M1 and M2. Vertical propagation of QTDW with westward phase is favored in the regions of weak eastward winds. However, as the eastward wind strengthens to velocity greater than critical velocity, amplitudes and vertical development of QTDW will be weakened (Salby 1981b). Thus, the favorable wind conditions strengthen W3 in the altitude regions of M1 and M2 and the strong eastward winds weaken W3 amplitudes in the regions in between. These vertically alternating conditions of zonal winds are found to be the potential reasons for the formation of double mode W3 structure in the MLT region. Vertically alternating structure of zonal winds observed in the MLT region could have been significantly influenced by gravity wave filtering from lower altitudes. As mentioned earlier, W3 gets developed after summer solstice, when the mesospheric easterly jet is strong. Prevailing westward winds at the lower altitudes favour vertical propagation of gravity waves, which are having eastward phases. Dissipation of these gravity waves, and consequent deposition of momentum, causes gradual weakening of westward winds with increase in altitude, its reversal to eastward winds and strengthening of eastward winds at higher altitudes as shown in Fig. 5a. This mechanism of gravity wave filtering and consequent formation of vertically alternating wind structure is proposed in earlier studies also (Palo et al. 1999). The QTDW at M2 can also filter the vertically propagating gravity waves so that it can modulate their momentum deposition in the lower thermosphere and imprint its signature at M1. Thus the analysis shows that the regions of M1 and M2 are characterized by weak eastward/westward winds, whereas the region of W3 weakening is characterized by strong eastward winds.

Meridional gradients in MLT temperature

Meridional temperature gradient plays a significant role in the vertical structure of zonal wind and vertical development of QTDW (Salby 1981a, b). Figure 5b shows meridional and vertical variations of temperature in January, for the 8 years of strong W3 events, in the MLT region. Lowest temperature of summer mesopause region can be seen in the altitude region between 80 and 90 km in southern hemisphere at south of 55° S. Meridional gradient in temperature, with increase from southern hemisphere high latitude regions to the equator, is seen

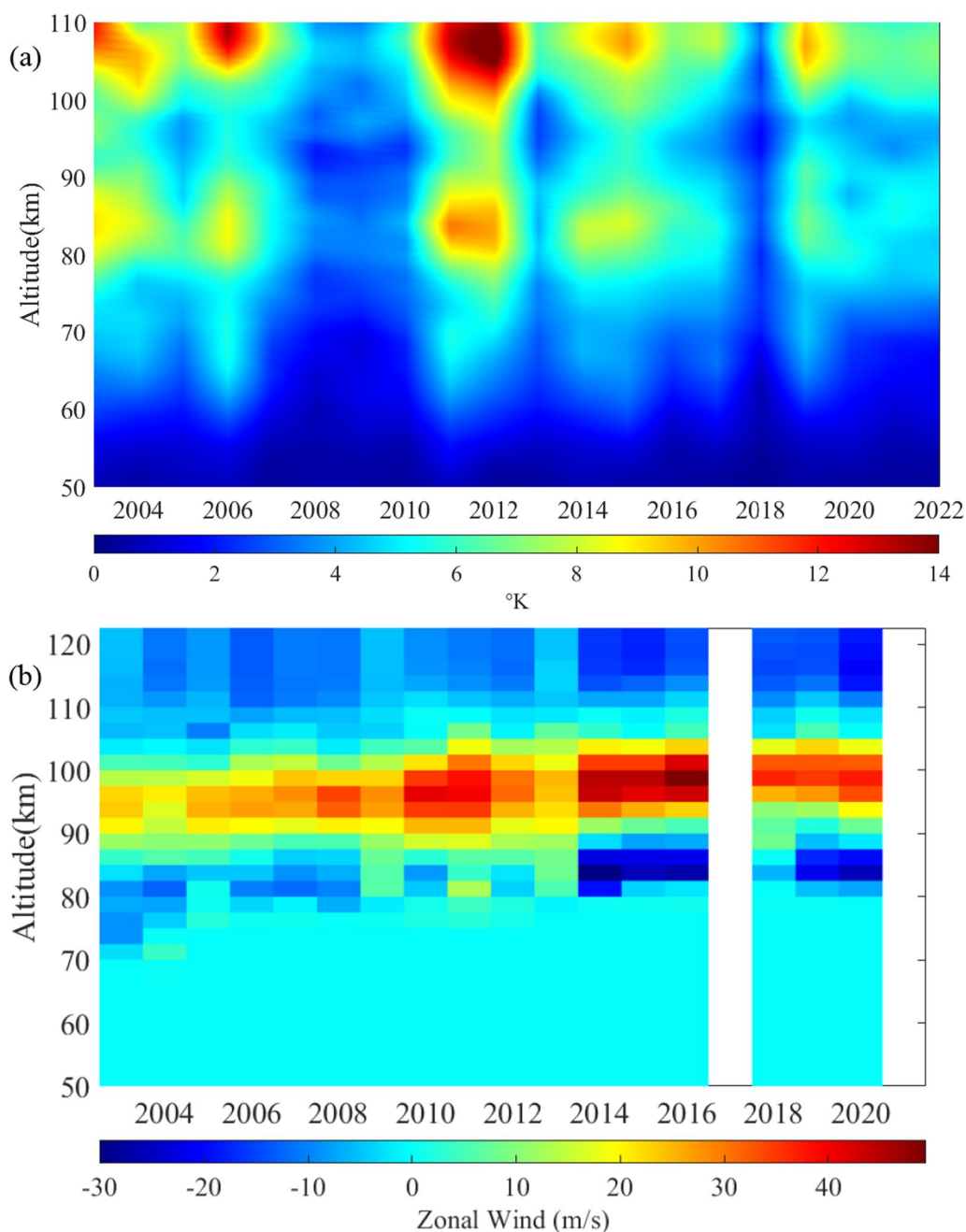


Fig. 4 **a** Vertical structure of W3 during the period from Jan 01 to Jan 31, over the latitude band between 50° S and 20° S, from 2003 to 2022 and **b** vertical structure of zonal wind in January over the same region from 2003 to 2020

at this altitude level. However, it is not observed to be so at higher altitude regions. Blue curve in Fig. 5c shows the vertical profile of meridional gradient in temperature averaged over the latitude band between 50° S and 20° S in January from the selected years of strong events. It is estimated as the increase in temperature over a latitudinal extent of 1° from south to north. Hence, the positive values of the gradient indicate increase in temperature

towards the Equator and vice versa. Black curve is same as that in Fig. 3c, which depicts the mean vertical profile of W3 amplitude, but for the altitude range from 70 to 110 km. It can be seen from the comparison between blue and black curves that the magnitude of horizontal temperature gradient is highest near the regions of M1 and M2 where W3 is strongest. Larger horizontal gradients in temperature causes stronger vertical shear

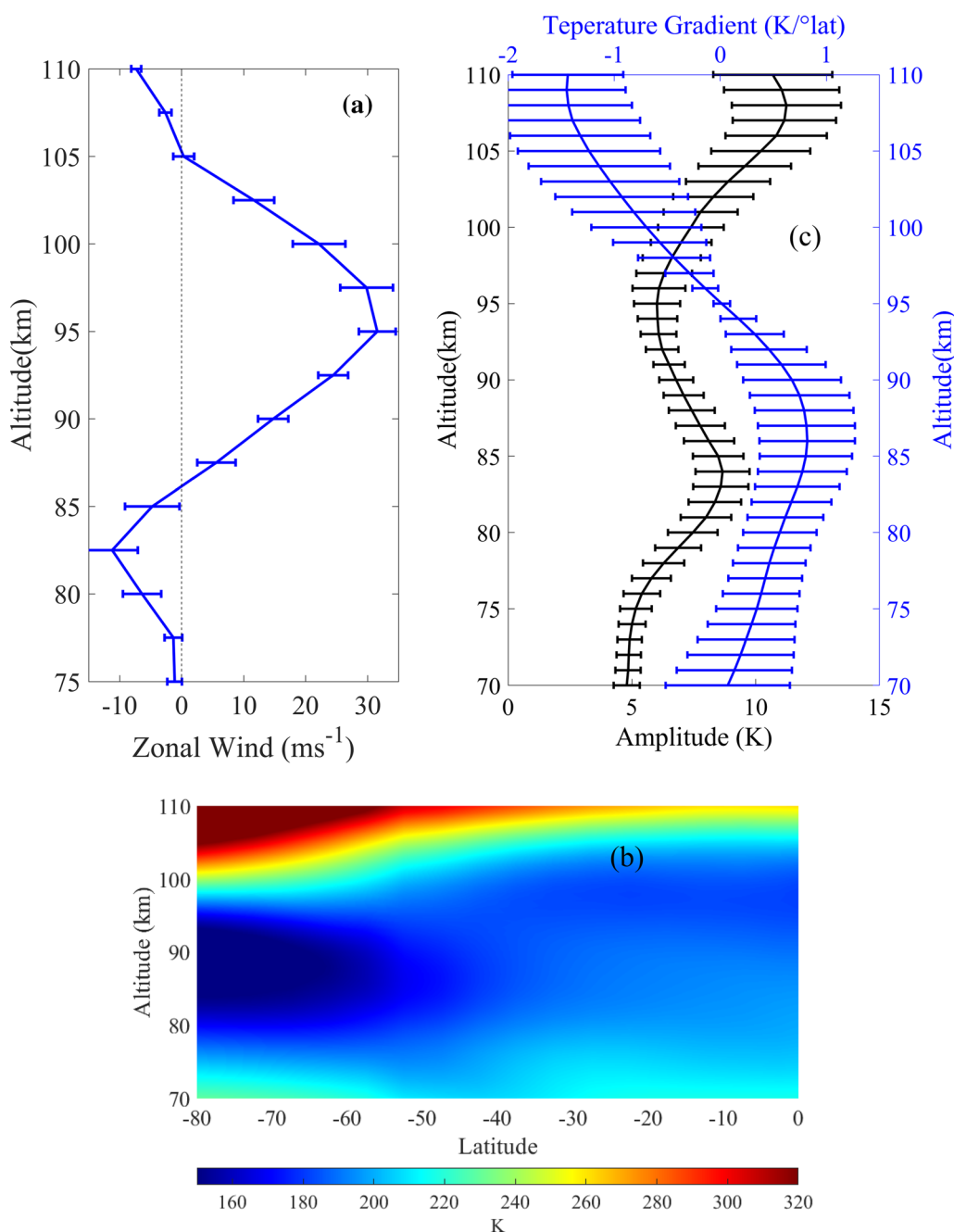


Fig. 5 **a** Mean vertical profile of zonal mean zonal wind, averaged over the latitude band between 50° S and 20° S, for the selected years. Positive values indicate eastward winds and negative values indicate westward winds. **b** Latitude–altitude variations of temperature in the MLT region in the month of January, from the selected years, using SABER measurements **c** Black curve is same as that in Fig. 3c, which depicts the mean vertical profile of W3 amplitude and blue curve shows the vertical profile of meridional gradient of temperature averaged over the latitude band 50° S–20° S in January in the selected years. Horizontal bars represent corresponding standard errors

in zonal winds. Thus, meridional gradient in temperature affects vertical shear of zonal winds and hence the associated baroclinic instability affects the strength of QTDW. In the altitude regions above 75 km, an increase in equatorward temperature gradient with altitude can

be observed as shown by the blue curve in Fig. 5c. This provides an eastward vertical shear in zonal wind (Salby 1981b), which causes weakening of prevailing westward wind and its gradual shift to eastward wind in the altitude regions above. This weak zonal wind provides conducive

conditions for the strengthening of QTDW and forms a peak in the regions of M2. However, further strengthening of eastward winds favored by the equatorward temperature gradient causes weakening of QTDW in the altitudes above M2 up to ~ 95 km. At this altitude level, strong eastward winds with amplitude close to 30 m/s are observed and it coincides with the regions of minimum QTDW amplitude. Above this level, meridional temperature gradient is observed to be poleward, which provides westward vertical wind shear in zonal winds (Salby 1981b). This westward wind shear causes gradual weakening of prevailing eastward winds and their reversal to westward winds in the higher altitudes. In addition, weakening of QTDW imparts westward momentum into the background and this also causes weakening of prevailing eastward winds. These lead to a condition of weak zonal winds, which is conducive for the vertical growth of QTDW and thus to the formation of QTDW peak in the altitude regions of M1. Thus the background winds and latitudinal gradients in temperature modulate the vertical structure of QTDWs.

Conclusions

Vertical structure of QTDW assumes importance, as far as the coupling between lower atmosphere and ionosphere is concerned. Asynoptic spectral analysis, with least square fitting method for spatially and temporally irregular sampling, carried out using two decades of temperature measurements from SABER show a multi-peak vertical structure of W3 QTDW in southern hemisphere mid-latitude in austral summer. Upper prominent peak is observed at 108 km, with W3 amplitude 11.24 ± 2.2 K, whereas the lower prominent peak is observed at 84 km, with W3 amplitude 8.66 ± 1.1 K. Genesis of this double peak vertical structure, which is seldom discussed in earlier reports, is investigated by examining the changes in wind and temperature fields. Regions of M1 and M2 experience weak eastward/westward winds, which are favorable for the strengthening and vertical growth of W3. However, altitude regions between M1 and M2 experience strong eastward winds, which cause weakening of W3. These vertical changes in amplitudes and direction of zonal winds are significantly modulated by the meridional gradients in temperature. Equatorward temperature gradients in the altitude regions below 95 km provide eastward wind shears. This leads to gradual weakening of westward winds in the lower levels with increase in altitudes, its reversal to eastward winds and further strengthening to maximum eastward winds at 95 km. Above this altitude level, poleward temperature gradients provide westward wind shears and hence lead to gradual weakening of eastward winds and its subsequent reversal to westward winds. Thus, the vertically

alternating temperature gradients lead to the conditions of weak zonal winds in the regions of M1 and M2 (where W3 peaks) and of strong eastward winds in the regions in between (where W3 weakens). In addition, gravity wave filtering also affects the zonal wind conditions in this region. Thus, the vertically alternating structure of zonal winds and meridional temperature gradient provide favorable and unfavorable conditions for the growth of W3 at different altitude levels in the MLT region and hence lead to the formation of a multi-peak vertical structure of W3. Further studies on multi-peak structure in the Northern Hemispheric mid-latitude during boreal summer may further shed light on the mechanisms through which it forms.

Acknowledgements

Authors acknowledge SABER team for providing data through <http://saber.gats-inc.com/data.php> and TIDI team for providing data through <http://timed.hao.ucar.edu/tidi/data.html>.

Author contributions

SSP and KKK conceived the idea and designed the study. SSP carried out the analysis and wrote the original manuscript. KKK did the supervision and review of the manuscript. SSP and KKK carried out the investigation and interpretation of results.

Funding

No.

Availability of data and materials

The data sets used in the study are available through <http://saber.gats-inc.com/data.php> and <http://timed.hao.ucar.edu/tidi/data.html>.

Declarations

Competing interests

The authors declare that they have no competing interests.

Author details

¹Space Physics Laboratory, Vikram Sarabhai Space Centre, Indian Space Research Organisation, Thiruvananthapuram, India.

Received: 3 March 2023 Accepted: 30 July 2023

Published online: 09 August 2023

References

- Gu SY, Li T, Dou X, Wu Q, Mlynczak MG, Russell JM (2013) Observations of quasi-two-day wave by TIMED/SABER and TIMED/TIDI. *J Geophys Res Atmos* 118:1624–1639. <https://doi.org/10.1002/jgrd.50191>
- Gu SY, Dou XK, Yang CY, Jia M, Huang KM, Huang CM, Zhang SD (2019) Climatology and anomaly of the quasi-two-day wave behaviors during 2003–2018 austral summer periods. *J Geophys Res Space Phys* 124:544–556. <https://doi.org/10.1029/2018JA026047>
- Guharay A, Batista PP, Clemesha BR, Schuch NJ (2013) Study of the quasi-two-day wave during summer over Santa Maria, Brazil using meteor radar observations. *J Atmos Sol Terr Phys*. <https://doi.org/10.1016/j.jastp.2012.10.005>
- Harris TJ, Vincent RA (1993) The quasi-two-day wave observed in the equatorial middle atmosphere. *J Geophys Res*. <https://doi.org/10.1029/93jd00380>
- He M, Chau JL, Forbes JM, Zhang X, Englert CR, Harding BJ, Immel TJ, Lima LM, Bhaskar Rao SV, Ratnam MV, Li G, Harlander JM, Marr KD, Makela JJ (2021) Quasi-2-day wave in low-latitude atmospheric winds as viewed from

- the ground and space during January–March, 2020. *Geophys Res Lett.* <https://doi.org/10.1029/2021GL093466>
- Huang YY, Zhang SD, Yi F, Huang CM, Huang KM, Gan Q, Gong Y (2013) Global climatological variability of quasi-two-day waves revealed by TIMED/SABER observations. *Ann Geophys* 31:1061–1075. <https://doi.org/10.5194/angeo-31-1061-2013>
- Jacobi C, Schminder R, Kürschner D (1997) The quasi 2-day wave as seen from D1 LF wind measurements over Central Europe (52°N, 15°E) at Collm. *J Atmos Sol Terr Phys* 59:1277–1286. [https://doi.org/10.1016/S1364-6826\(96\)00170-8](https://doi.org/10.1016/S1364-6826(96)00170-8)
- Jacobi C, Schminder R, Kürschner D (1998) Non-linear interaction of the quasi 2-day wave and long-term oscillations in the summer midlatitude mesopause region as seen from LF D1 wind measurements over Central Europe (Collm, 52°N, 15°E). *J Atmos Sol Terr Phys* 60:1175–1191. [https://doi.org/10.1016/S1364-6826\(98\)00076-5](https://doi.org/10.1016/S1364-6826(98)00076-5)
- Killeen TL, Skinner WR, Johnson RM, Edmonson CJ, Wu Q, Niciejewski RJ, Grassl HJ, Gell DA, Hansen PE, Harvey JD, Kafkalidis JF (1999) TIMED Doppler interferometer (TIDI). Optical spectroscopic techniques and instrumentation for atmospheric and space research III. SPIE, Bellingham. <https://doi.org/10.1117/12.366383>
- Kumar KK, Subrahmanyam KV, Mathew SS, Koushik N, Ramkumar G (2018) Simultaneous observations of the quasi 2-day wave climatology over the low and equatorial latitudes in the mesosphere lower thermosphere. *Clim Dyn.* <https://doi.org/10.1007/s00382-017-3916-2>
- Li Y, Chen G, Zhang S, Gong W, Ma Z, Huang K, Gong Y (2021) Effect of semidiurnal lunar tides modulated by quasi-2-day wave on equatorial electrojet during three sudden stratospheric warming events. *Geophys Res Lett.* <https://doi.org/10.1029/2021GL095352>
- Moudden Y, Forbes JM (2014) Quasi-two-day wave structure, interannual variability, and tidal interactions during the 2002–2011 decade. *J Geophys Res* 119:2241–2260. <https://doi.org/10.1002/2013JD020563>
- Muller HG, Kingsley SP (1974) Long period meteor wind oscillations. *J Atmos Terr Phys* 36:1933–1943. [https://doi.org/10.1016/0021-9169\(74\)90180-9](https://doi.org/10.1016/0021-9169(74)90180-9)
- Nguyen VA, Palo SE, Lieberman RS, Forbes JM, Ortland DA, Siskind DE (2016) Generation of secondary waves arising from nonlinear interaction between the quasi 2 day wave and the migrating diurnal tide. *J Geophys Res.* <https://doi.org/10.1002/2016JD024794>
- Palo SE, Roble RG, Hagan ME (1999) Middle atmosphere effects of the quasi-two-day wave determined from a general circulation model. *Earth Planets Space* 51:629–647. <https://doi.org/10.1186/BF03353221>
- Pancheva DV (2006) Quasi-2-day wave and tidal variability observed over Ascension Island during January/February 2003. *J Atmos Sol Terr Phys.* <https://doi.org/10.1016/j.jastp.2005.02.028>
- Pancheva D, Mitchell NJ, Manson AH, Meek CE, Jacobi C, Portnyagin Y, Merzlyakov E, Hocking WK, MacDougall J, Singer W, Igarashi K, Clark RR, Riggins DM, Franke SJ, Kürschner D, Fahrutdinova AN, Stepanov AM, Kashcheyev BL, Oleynikov AN, Muller HG (2004) Variability of the quasi-2-day wave observed in the MLT region during the PSMOS campaign of June–August 1999. *J Atmos Sol Terr Phys* 66:539–565. <https://doi.org/10.1016/j.jastp.2004.01.008>
- Pancheva D, Mukhtarov P, Siskind DE (2018) Climatology of the quasi-2-day waves observed in the MLS/Aura measurements (2005–2014). *J Atmos Sol Terr Phys* 171:210–224. <https://doi.org/10.1016/j.jastp.2017.05.002>
- Pfister L (1985) Baroclinic instability of easterly jets with applications to the summer mesosphere. *J Atmos Sci.* [https://doi.org/10.1175/1520-0469\(1985\)042%3c0313:BOEJW%3e2.0.CO;2](https://doi.org/10.1175/1520-0469(1985)042%3c0313:BOEJW%3e2.0.CO;2)
- Plumb RA (1983) Baroclinic instability of the summer mesosphere: a mechanism for the quasi-two-day wave? *J Atmos Sci* 40:262–270. [https://doi.org/10.1175/1520-0469\(1983\)040%3c0262:BIOTSM%3e2.0.CO;2](https://doi.org/10.1175/1520-0469(1983)040%3c0262:BIOTSM%3e2.0.CO;2)
- Russell JM III, Mlynczak MG, Gordley LL, Tansock JJ Jr, Esplin RW (1999) Overview of the SABER experiment and preliminary calibration results. Optical spectroscopic techniques and instrumentation for atmospheric and space research III. SPIE, Bellingham, p 277. <https://doi.org/10.1117/12.366382>
- Salby ML (1981a) The 2-day wave in the middle atmosphere: observations and theory. *J Geophys Res* 86:9654. <https://doi.org/10.1029/jc086ic10p09654>
- Salby ML (1981b) Rossby normal modes in nonuniform background configurations. Part I: simple fields. *J Atmos Sci* 38(9):1803–1826. [https://doi.org/10.1175/1520-0469\(1981\)038%3c1803:RNMINB%3e2.0.CO;2](https://doi.org/10.1175/1520-0469(1981)038%3c1803:RNMINB%3e2.0.CO;2)
- Salby ML, Roper RG (1980) Long-period oscillations in the meteor region. *J Atmos Sci* 37:237–244. [https://doi.org/10.1175/1520-0469\(1980\)037%3c0237:lpoitm%3e2.0.co;2](https://doi.org/10.1175/1520-0469(1980)037%3c0237:lpoitm%3e2.0.co;2)
- Suresh Babu V, Kishore Kumar K, John SR, Subrahmanyam KV, Ramkumar G (2011) Meteor radar observations of short-term variability of quasi 2 day waves and their interaction with tides and planetary waves in the mesosphere-lower thermosphere region over Thumba (8.5N, 77E). *J Geophys Res Atmos.* <https://doi.org/10.1029/2010JD015390>
- Thayaparan T, Hocking WK, MacDougall J (1997) Amplitude, phase, and period variations of the quasi 2-day wave in the mesosphere and lower thermosphere over London, Canada (43°N, 81°W), during 1993 and 1994. *J Geophys Res Atmos* 102:9461–9478. <https://doi.org/10.1029/96jd03869>
- Tunbridge VM, Sandford DJ, Mitchell NJ (2011) Zonal wave numbers of the summertime 2 day planetary wave observed in the mesosphere by EOS Aura Microwave Limb Sounder. *J Geophys Res Atmos.* <https://doi.org/10.1029/2010JD014567>
- Vincent RA (2015) The dynamics of the mesosphere and lower thermosphere: a brief review. *Prog Earth Planet Sci.* <https://doi.org/10.1186/s40645-015-0035-8>
- Ward WE, Wang DY, Solheim BH, Shepherd GG (1996) Observations of the two-day wave in WINDII data during January, 1993. *Geophys Res Lett* 23(21):2923–2926. <https://doi.org/10.1029/96GL02897>
- Wu DL, Hays PB, Skinner WR (1995) A least squares method for spectral analysis of space-time series. *J Atmos Sci* 52:3501–3511. [https://doi.org/10.1175/1520-0469\(1995\)052%3c3501:ALSMF%3e2.0.CO;2](https://doi.org/10.1175/1520-0469(1995)052%3c3501:ALSMF%3e2.0.CO;2)
- Yue J, Liu HL, Chang LC (2012a) Numerical investigation of the quasi 2 day wave in the mesosphere and lower thermosphere. *J Geophys Res Atmos.* <https://doi.org/10.1029/2011JD016574>
- Yue J, Wang W, Richmond AD, Liu HL (2012b) Quasi-two-day wave coupling of the mesosphere and lower thermosphere-ionosphere in the TIME-GCM: two-day oscillations in the ionosphere. *J Geophys Res Sp Phys.* <https://doi.org/10.1029/2012JA017815>
- Yue J, Wang W, Ruan H, Chang LC, Lei J (2016) Impact of the interaction between the quasi-2 day wave and tides on the ionosphere and thermosphere. *J Geophys Res Sp Phys* 121:3555–3563. <https://doi.org/10.1002/2016JA022444>
- Zhou QH, Sulzer MP, Tepley CA (1997) An analysis of tidal and planetary waves in the neutral winds and temperature observed at low-latitude E region heights. *J Geophys Res Sp Phys* 102(A6):11491–11505. <https://doi.org/10.1029/97JA00440>

Publisher's Note

Springer Nature remains neutral with regard to jurisdictional claims in published maps and institutional affiliations.

Submit your manuscript to a SpringerOpen® journal and benefit from:

- Convenient online submission
- Rigorous peer review
- Open access: articles freely available online
- High visibility within the field
- Retaining the copyright to your article

Submit your next manuscript at ► [springeropen.com](https://www.springeropen.com)